Quantifying Parasitic Losses from Metal Scattering Structures in Solar Cells: How Uncertainty in Optical Constants Affects Simulation Results

P. Pearce[†], A. Mellor[†], N. Ekins-Daukes[†‡]

[†] Department of Physics, Imperial College London, South Kensington Campus, London, SW7 2AZ, UK
[‡] School of Photovoltaic and Renewable Energy Engineering, UNSW, Sydney, NSW 2052, Australia

***Abstract* — The optical constants of many metals commonly used in solar cells, e.g. as contacts or for light trapping structures, are not documented consistently in the literature, with different sources giving different values. In the case of metallic structures designed to improve absorption in a solar cell junction, the use of data from different sources can give strongly varying results for the effectiveness of nanophotonic light-trapping structures. The trade-off between diffraction into more oblique orders in the junction, enhancing absorption in the photovoltaic material, and the number of photons absorbed parasitically in the metal means small differences in the optical constants can lead to different very conclusions about the EQE and J_{SC}. This work documents the different optical constants for silver, aluminium, gold and titanium from several sources, the effect this has on plasmon quality factors, and quantifies the effect on modelling outcomes by considering the optimization of a test structure using a grid of metal nanodisks on the front surface of a thinned-down GaAs cell. Finally, we consider the effect for a structure previously predicted to give a very high J_{SC} for a solar cell with an ultra-thin GaAs layer.**

***Index Terms* — light-trapping, ultrathin cells, plasmonics, optical modelling**

I. Introduction

Arrays of metal nanoparticles, other diffracting structures using metal grids or perforated films, and randomly arranged scattering nanoparticles [1]–[8] have all been investigated as methods for improving absorption in solar cell junctions using plasmonic effects and scattering into more oblique orders. Since metals are lossy, it can be unclear how any measured increase in total absorption observed due to the presence of the light trapping structure is distributed [9], unless a full device is manufactured so quantum efficiency can be measured. In this case, simulations are frequently used to determine the expected EQE and J_{SC}. Obviously, absorption in the metal is parasitic and should be considered a loss, and thus in order to accurately predict solar cell performance it is critical to correctly evaluate absorption in the target layer and in any parasitically absorbing layers, and not just total absorption.

A complicating factor in obtaining accurate simulation results is the uncertainty regarding the correct optical constants for commonly used metals such as gold, silver and titanium. Different sources often report significantly different optical constants for the same material, depending on the experimental method or model used to obtain the optical constants and the type of material measured (e.g. bulk or evaporated). Even metals grown by nominally similar methods can have different optical properties [10], and results may be affected by layer thicknesses and possible effects from surface layers (e.g. some metals will oxidise or tarnish if exposed to air). There appears to be a bias towards optical constants which give the most optimal results with little indication that these are the most appropriate data available; this was discussed in [11] for the case of silver optical constant data from Johnson & Christy [12]. This data has low κ (and thus low absorption) and high

TABLE I

SOURCES USED FOR OPTICAL CONSTANT DATA, THE LABELS BY WHICH THEY ARE REFERRED TO THROUGHOUT THIS WORK, WHICH OF THE METALS CONSIDERED HERE CAN BE FOUND IN EACH REFERENCE, AND A BRIEF SUMMARY OF THE METHOD BY WHICH THE OPTICAL CONSTANTS WERE MEASURED OR MODELLED.

Reference	Label	Metals	Method
Hagemann et al. [19]	Hag	Al, Ag, Au	Transmittance measurements of vacuum-evaporated films/Kramers-Kronig analysis
Jiang et al. [11]	Jia	Ag	Variable-angle spectroscopic ellipsometry of overlayer-protected films
Johnson & Christy [12]	J&C	Ag, Au, Ti	Reflection and transmission measurements on vacuum evaporated films
Lynch et al. [20]	Lyn	Ti	Absorptivity/reflectivity measurements of polycrystalline Ti/Kramers-Kronig analysis
McPeak et al. [10]	McP	Ag, Al, Au	Variable-angle spectroscopic ellipsometry of template-stripped samples
Olmon et al. [21]	Olm	Au*	Variable-angle spectroscopic ellipsometry of evaporated gold
Palik [15]	Pal	Ag, Al, Au, Ti	Various
Rakić et al. [22]	Rak-BB	Ag, Al, Au, Ti	Brendel-Bormann model fit to available experimental data
Rakić et al. [22]	Rak-LD	Ag, Al, Au, Ti	Lorentz-Drude model fit to available experimental data
Werner et al. [23]	Wer-R	Ag, Au, Ti	Reflection electron energy-loss spectroscopy (REELS)
Werner et al. [23]	Wer-D	Ag, Au, Ti	Density functional theory (DFT) calculations

* Olmon et al. [21] measured the optical constants of evaporated gold, template-stripped gold, and single-crystal gold; the values used here are for evaporated gold.

localized surface plasmon (LSP) and surface plasmon polariton (SPP) quality factors compared to other data sources (see Fig. 2). Despite the availability of newer data and the large instrumental error reported in [12], this data continues to be widely used (e.g. in [4]–[6], [13]). Similar issues can readily be observed for other common metals including gold and titanium by comparing literature values. In this work, four commonly-used metals are considered: silver, aluminium, gold, and titanium. In order to assess how use of different optical constants affect the simulations, each data set is used to optimize a simple solar cell-like optical structure in terms of optimal size and period of a scattering nanodisk array. In the cases of three of the four metals (all expect Al), different optical constants lead to significantly different optimal arrangements for maximum absorption and thus J_{SC}.

II. Methodology

A. Optical constants sources

Table I shows the different sources used for complex refractive index $n + i\kappa$ of Ag, Al, Au and Ti, with references provided and the labels used throughout clarified. Fig. 2a shows the refractive index n and extinction coefficient κ for each source. Not all sources have optical constant data for each of the metals considered here, and thus the number of data sets varies per metal (of course, more sources than those listed here

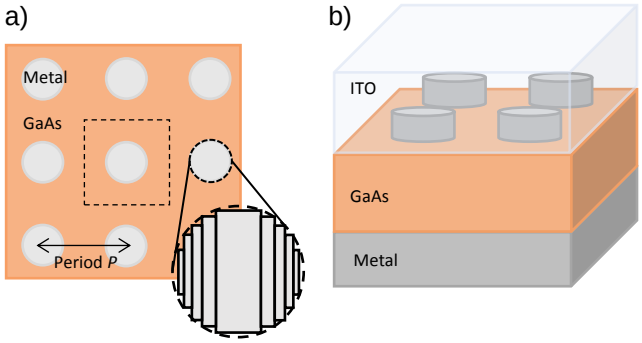

Fig. 1. Schematic of the solar cell structure used for the simulations: a) Top-down view, with one unit cell outlined. The inset shows how the disks are built up in the RCWA method. b) Side view.

are available). Although Palik's Handbook of Optical Constants takes data from other sources, it is included here as a distinct source as it is very frequently cited and often the principal source when optical constant data is required. For each source, the LSP Q factor was calculated; this is defined in terms of the dielectric function $\varepsilon_1 + i\varepsilon_2$ as [11], [14]:

$$LSPQ = \frac{-\varepsilon_1}{\varepsilon_2} = \frac{|n^2 - \kappa^2|}{2n\kappa} \quad (1)$$

in the region where ε_1 is negative. The field enhancement in a material depends on ε_1, while the absorption (loss) depends on ε_2, and thus both quantities affect the optical performance.

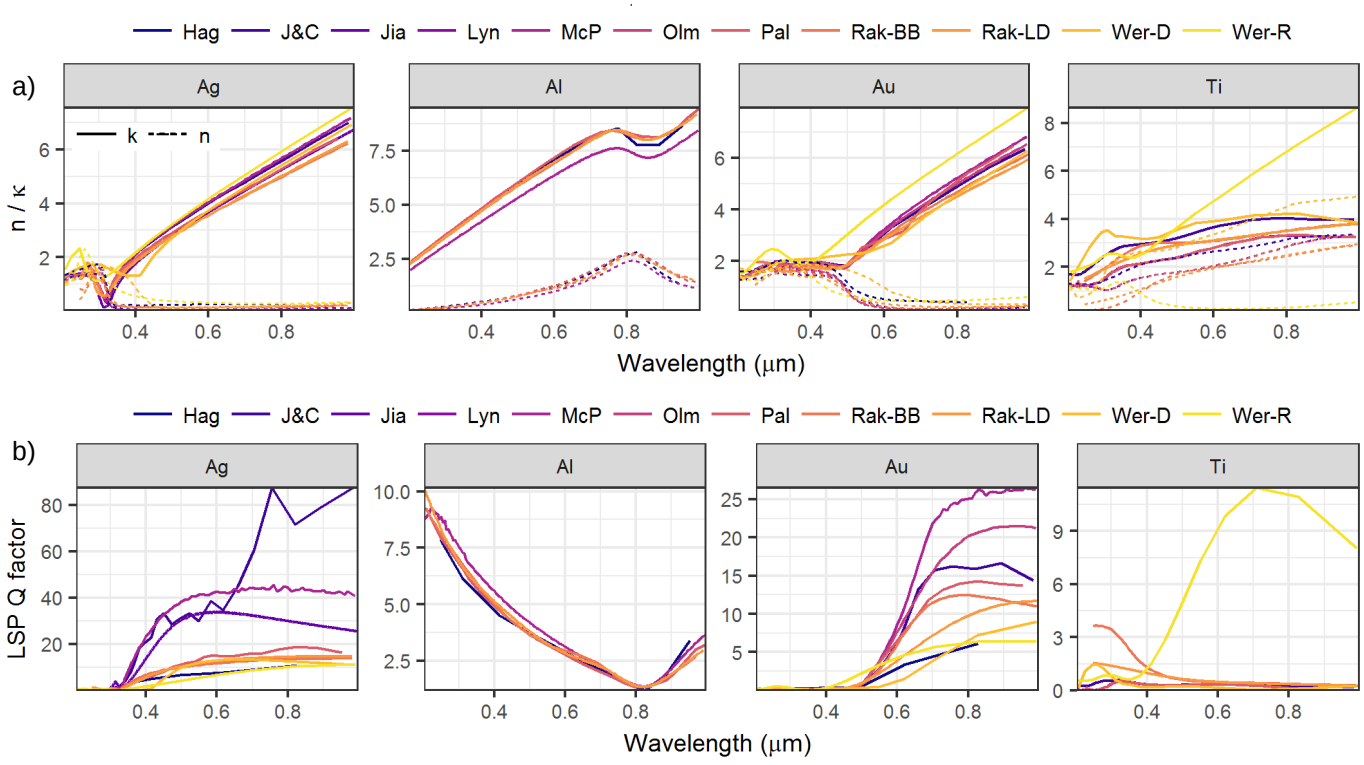

Fig. 2. a) n and κ for Ag, Al, Au and Ti, from different sources. Values were taken either directly from the published work (see Table I) or from [24]. b) Localised surface plasmon (LSP) quality factor.

B. Simulated structures

To quantify the light-trapping benefit from a metallic nanostructure, we consider a considerably thinned-down GaAs junction with a thickness of 50 nm (compared to a 'normal' cell thickness of around 1 μm); this is so that the light-trapping can, in theory, have a significant benefit. The GaAs is covered by 60 nm of indium tin oxide (ITO), which acts as an anti-reflection coating (ARC) and encapsulates the metal nanoparticles. Its thickness was chosen as simulations showed 60 nm to be near the optimum thickness for minimizing reflection for these configurations. The optical constant data for was taken from [15] for GaAs and [16] for ITO. The metal NPs are disk-shaped pillars, and are arranged in a square grid as shown in Fig. 1. To reduce the parameter space, the height of the pillars (20 nm), ITO thickness (60 nm), and GaAs thickness (50 nm) were kept constant, while the period of the array and metal coverage (i.e. radius of the disks) was varied. The cell has a metal back mirror (made of the same metal as the NPs), which is considered to be a semi-infinite transmission medium in the simulations. The metal coverage fraction is defined as:

$$C = \frac{\text{area covered by metal}}{\text{total area}} = \frac{\pi r^2}{P^2} \qquad (2)$$

when the cell is viewed as in Figure 1a, where r is the nanodisk fradius and P is the array period. Thus the maximum coverage fraction before the disks start to overlap is $\pi/4$, when $r = P/2$.

C. Simulation method

Rigorous coupled-wave analysis (RCWA), sometimes referred to as the Fourier modal method (FMM), is a method for calculating scattering effects due to periodic structures. This is done by defining a structure which is periodic in two orthogonal lateral directions x and y. The electromagnetic field and permittivity at a particular height z perpendicular to the lateral directions can then be represented in terms of Fourier series, and a system of differential equations following from Maxwell's equations can be developed to solve for the field's Fourier coefficients as it propagates through the structure. Knowledge of the electric and magnetic field amplitudes in each diffraction order allows the absorbed and transmitted power to be calculated using the Poynting vector $\boldsymbol{S} = \boldsymbol{E} \times \boldsymbol{H}$. The method requires that only a limited number of Fourier orders are retained for the calculation; here, 21 orders along the x and y directions are retained (441 orders in total), after convergence tests showed this to be a sufficient number. There are many implementations of RCWA available in different programming languages; GD-Calc (Grating Diffraction Calculator) [17], a MATLAB-based simulation tool, was used to calculate the results presented in this work. Since only rectangular blocks can be used, the nanodisks must be built up out of strips; the inset in Fig. 1a illustrates this using nine strips. In the simulations, the disks were built up of 201 strips.

The J_{SC} values given in the subsequent sections were calculated using:

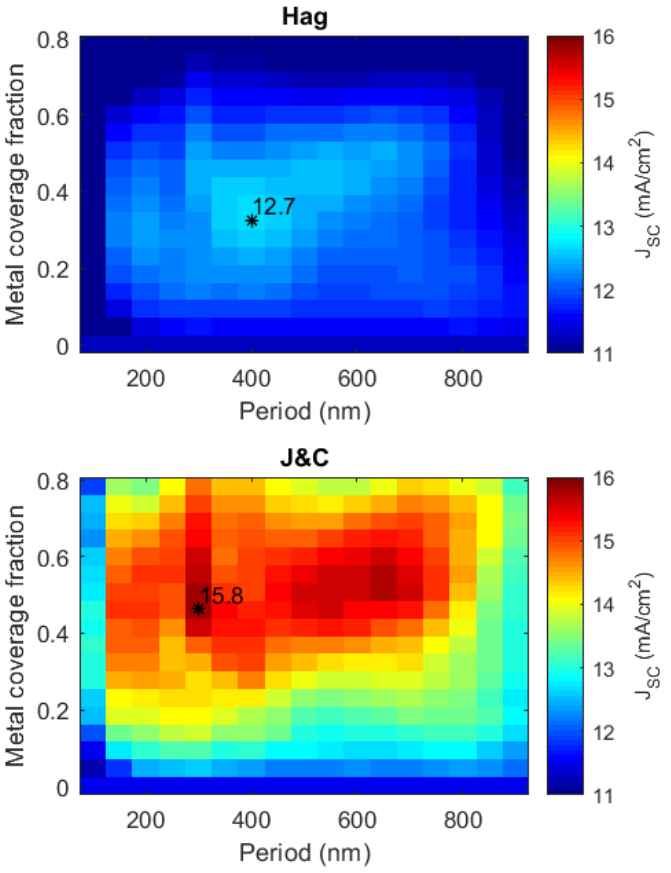

Fig. 3. Predicted short-circuit current JSC as a function of array period P and metal coverage fraction C for the structure shown in Fig. 1 using two different sets of optical constant data (Hag and J&C) for silver. The ✷ indicates the location of the maximum J_{SC}, which is indicated in both cases.

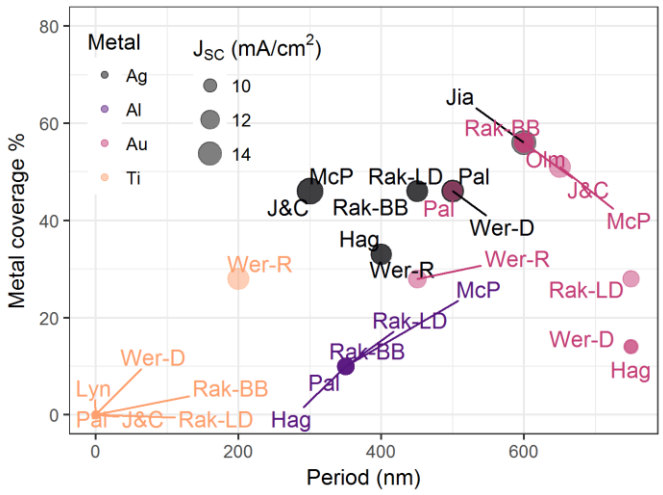

Fig. 4. Location of the optimum configuration of nanodisks in terms of metal coverage and period for each optical constant source, corresponding to the points marked with ✷ for the two illustrative cases in Fig. 3. The different colours indicate different metals, and the size of the point indicates the relative size of each maximum. The point (0, 0) (i.e. 0 % metal coverage) means no nanoparticles are present, so the structure is bare GaAs with an ITO ARC and metal back mirror.

$$q \int \phi(\lambda) A(\lambda) d\lambda \qquad (3)$$

Where q is the elementary charge, ϕ the spectral photon flux (calculated from a standard ASTMG173 reference spectrum [18]), and A the fraction of photons absorbed in the GaAs layer (an IQE of 100% is assumed) at normal incidence. For both structures, simulations and J_{SC} calculations were carried out over the wavelength range 300-900 nm.

D. Optimization

A simple grid search was performed covering the full parameter space of metal coverage C and array period P using each set of optical constant values. With the resolution chosen, this meant around 300 simulations had to be performed in each case, and thus a High Performance Computing cluster was used.

III. Optical Constants & Figures of Merit

Fig. 2 shows the optical constants and LSP Q factor for the different sources, grouped by metal. With the exception of Ti, the optical constants (Fig. 2a) for the same metal appear to follow the same trends, with some variation in magnitudes. However, these apparently small variations can lead to very large variations in the calculated LSP Q factor (Fig. 2b). The J&C data is a clear outlier for silver, and McP gives the highest Q factor for gold, although the other sources also vary considerably. Unlike the other metals considered, the optical constants for aluminium were consistent across sources. For Ti, both the complex refractive index and thus, unsurprisingly, the LSP Q factor vary strongly depending on source, with the Wer-R data having a Q factor more than 25 times higher than any other source around 0.7 µm.

IV. Predicted J_{SC} and EQE

An example of the outcome of the grid searches for two sets of silver optical constant data is shown in Fig. 3. The metal coverage and array period giving the maximum J_{SC} for each source are shown in Fig. 4, and detailed results on the optimum for each source are given in Table III. In each case, the source with the highest LSP Q factors also gives the highest optimum

TABLE II

Best and worst outcomes, and the mean, using the nanodisk arrangements highlighted in Table III (i.e. those which give the highest overall J_{SC} per metal out of all sources considered). Al is not included as there is no significant difference between sources.

		Best		Worst		Mean
Ag	J_{SC} (mA/cm^2)	J&C	15.8	Wer-R	12.6	13.7 (1.1)
	A (%)		58.3		53.5	55.1 (2.0)
Au	J_{SC} (mA/cm^2)	McP	12.9	Wer-D	9.89	11.5 (1.1)
	A (%)		57.3		40.7	51.1 (6.3)
Ti	J_{SC} (mA/cm^2)	Wer-R	13.1	Lyn	9.00	9.66 (1.4)
	A (%)		58.0		34.4	38.0 (8.2)

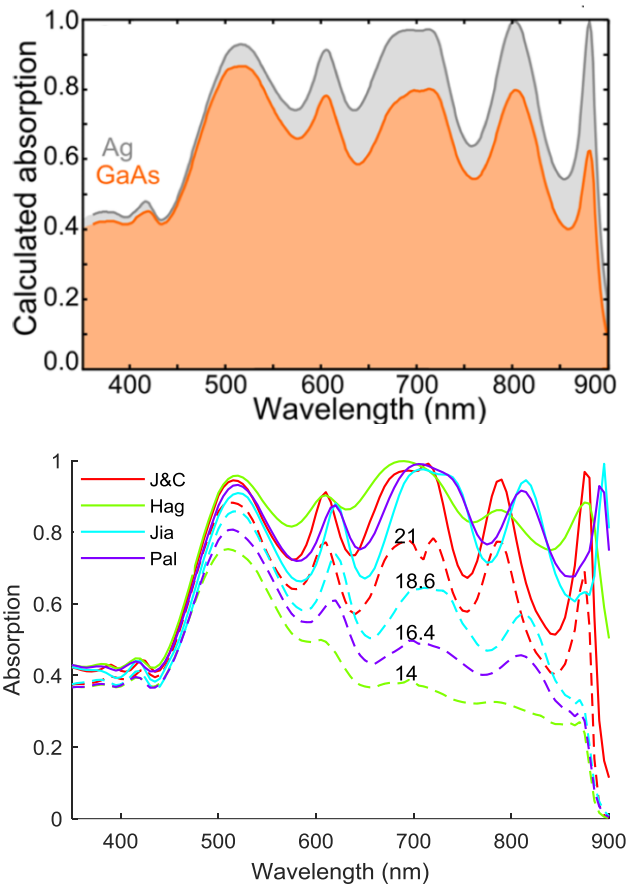

Fig. 5. Top: Calculated absorption in the total metal nanogrid + GaAs structure and in the GaAs layer. Figure from [4]. Bottom: same, recalculated using our RCWA implementation for four different optical constant sources. The solid lines show total absorption while the dashed lines show absorption in the GaAs layer only. The labels indicate the predicted J_{SC} due to absorption in the GaAs layer for each source.

J_{SC}. The spread of optimal solutions predicted using different sources is evident for all metals except Al, although there are also coinciding points for Ag, Au and Ti. For Ti, six out of seven sources predict that a nanodisk array of the type considered here does not offer any potential for J_{SC} improvement, while Wer-R predicts a 15 % increase relative to the J_{SC} without nanodisks. Clearly, the choice of optical constant source has a significant effect when exploring possible arrangements for nanometallic structures in order to decide on an optimum for device fabrication. Fig. 6 shows the results of all the simulations in terms of J_{SC} vs. metal coverage; for each source, there is a clear trend, but these diverge significantly between sources for all metals except Al.

Table II shows the outcomes when the optimal nanodisk arrangement for the source giving the highest Q factors and J_{SC}s for each metal (values highlighted in bold Table III) is considered for other optical constant sources. For Ag, Au and Ti, the percentage reduction between the best J_{SC} and the mean are 13%, 11%, and 26%, indicating that unless the actual optical

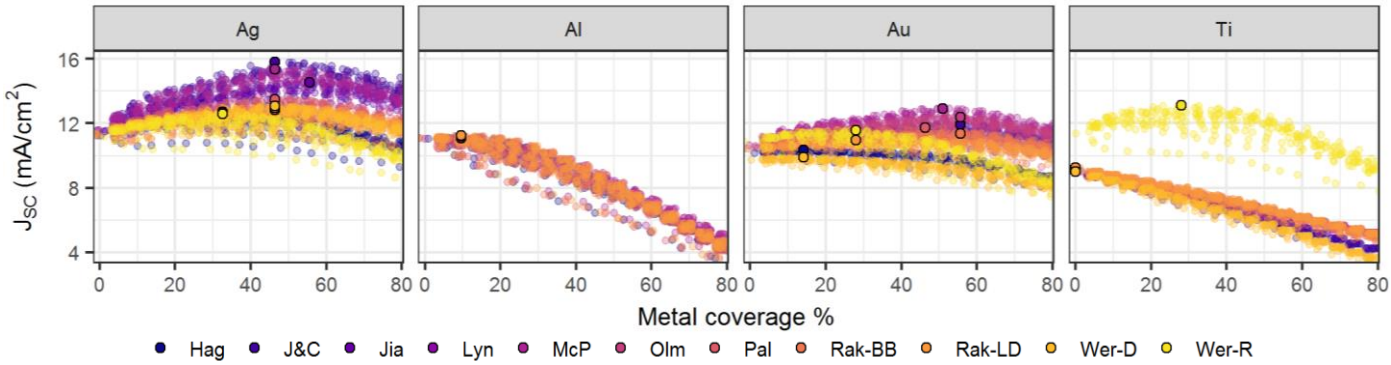

Fig. 6. J_{SC} versus metal coverage C, showing the results of all the simulations (points are jittered slightly along the x-axis since C increases in discrete steps). Different colours represent different sources, and the point corresponding to the maximum J_{SC} is outlined in black for each source (for Al, all these points coincide).

TABLE III

DETAILED SIMULATION RESULTS SHOWING THE J_{SC} WITHOUT NANOPARTICLES (J_0), THE OPTIMAL ARRANGEMENT IN TERMS OF PERIOD P AND METAL COVERAGE C LEADING TO MAXIMUM SHORT-CIRCUIT CURRENT J_{MAX}. THE LAST FOUR COLUMNS ARE THE PERCENTAGE AVERAGE ABSORPTION OVER THE RANGE 300-900 NM, AND THE AVERAGE PERCENTAGE OF THOSE PHOTONS ABSORBED IN THE GAAS, THE NANOPARTICLES LAYER (NP) AND THE BACK MIRROR. THE SOURCE GIVING THE HIGHEST J_{SC} IS IN BOLD FOR EACH METAL.

Source	J_0	P_{opt}/C_{opt}	J_{max}	A_{avg}	GaAs	NP	Back
Silver (Ag)							
Hag	11.3	400/0.33	12.7	53	77	17	14
Jia	11.5	600/0.56	14.5	56	79	16	5
J&C	**11.5**	**300/0.46**	**15.8**	**58**	**83**	**13**	**2**
McP	11.6	300/0.46	15.4	58	81	14	3
Pal	11.3	500/0.46	13.5	54	77	17	9
Rak-BB	11.3	450/0.46	12.8	53	76	18	10
Rak-LD	11.3	450/0.56	13.0	53	77	18	9
Wer-D	11.3	500/0.33	13.1	56	73	22	11
Wer-R	11.2	400/0.33	12.6	54	75	20	15
Aluminium (Al)							
Hag	11.0	350/0.10	11.2	45	83	11	40
McP	11.0	350/0.10	11.1	45	83	11	38
Pal	11.1	350/0.10	11.2	45	84	11	41
Rak-BB	11.1	350/0.10	11.2	45	84	11	39
Rak-LD	**11.1**	**350/0.10**	**11.2**	**45**	**84**	**11**	**39**
Gold (Au)							
Hag	10.1	750/0.14	10.4	42	84	12	33
J&C	10.5	600/0.56	12.0	56	65	30	16
McP	**10.6**	**650/0.51**	**12.9**	**57**	**69**	**26**	**13**
Olm	10.6	600/0.56	12.4	57	66	29	14
Pal	10.5	500/0.46	11.7	54	68	27	17
Rak-BB	10.4	600/0.56	11.4	55	64	31	17
Rak-LD	10.4	750/0.28	11.0	46	79	17	22
Wer-D	9.7	750/0.14	9.9	41	83	13	40
Wer-R	10.9	450/0.28	11.6	51	73	22	23
Titanium (Ti)							
J&C	9.1	0/0	9.1	35	95	5	106
Lyn	9.0	0/0	9.0	34	95	5	106
Pal	9.0	0/0	9.0	34	95	5	106
Rak-BB	9.2	0/0	9.2	35	95	5	95
Rak-LD	9.2	0/0	9.2	35	95	5	94
Wer-D	9.0	0/0	9.0	34	95	5	121
Wer-R	**11.4**	**200/0.28**	**13.1**	**58**	**71**	**23**	**12**

constants of materials used in a device match those used in simulations very closely, the solar cell performance may be significantly worse than predicted by simulations.

Table II also shows that while the predicted J_{SC} may vary considerably, this is not necessarily reflected by changes in the total absorption. This indicates that when comparing modeling and experimental results, overall absorption may match the experiment even if the balance between parasitic absorption and absorption enhancement in the target layer was not simulated correctly.

V. CONSEQUENCES FOR SOLAR CELL MODELLING

As discussed in the introduction, many published simulation results continue to use silver data from J&C, which gives low parasitic absorption. An example is the multiresonant metallic nanogrid structure reported in [4]. This paper predicts a J_{SC} of 21.6 mA/cm^2 for an ultra-thin GaAs layer of 25 nm, using a biperiodic nanogrid of thickness 20nm and period 500nm (full details of the structure can be found in [4]). Fig. 5 shows calculated total absorption and absorption in the GaAs as reported in [4], and calculated using our RCWA implementation for four different optical constant sources. When using J&C data, the results both in terms of absorption profile and predicted J_{SC} (21 mA/cm^2) are very similar. However, using other sources significantly reduces the predicted J_{SC}. Jiang et al. [11] (labelled 'Jia' here) measured the optical constants of silver specifically to address the problem with J&C data and provide new, realistic optical constants for evaporated silver; using these optical constants gives a J_{SC} 11 % lower than that predicted in [4]. Other sources given even worse outcomes, with Hagemann data giving a predicted a J_{SC} of only 14 mA/cm^2. All the data sources give similar resonant peaks to the J&C data in the *total* absorption spectrum, while the fraction absorbed in GaAs varies significantly.

VI. CONCLUSION

The effectiveness of periodic light-trapping structures which contain metals is significantly affected by the exact optical constants of these metals, and thus obtaining realistic optical

constant data is key to matching experiment and simulation. When simulations are being used to design an optimal structure, using inaccurate optical constants can lead to an incorrect optimal structure being identified. Wherever possible, optical constants of metals deposited in the same way as would be done during device manufacture should be measured through e.g. ellipsometry, taking care to avoid effects due to surface layers, tarnishing or oxidization. If it is not possible to obtain the optical constants directly, accurate data with low measurement uncertainty from metals which were deposited in a similar way and with similar thickness should be used.

ACKNOWLEDGEMENTS

P. Pearce would like to acknowledge EPSRC CASE sponsorship from IQE plc., and the Imperial College High Performance Computing Service for the computational resources provided.

REFERENCES

[1] C. F. Guo, T. Sun, F. Cao, Q. Liu, and Z. Ren, "Metallic nanostructures for light trapping in energy-harvesting devices," *Light Sci. Appl.*, vol. 3, no. 11, pp. 1–12, 2014.

[2] M. A. Green and S. Pillai, "Harnessing plasmonics for solar cells," *Nat. Photonics*, vol. 6, no. 3, pp. 130–132, 2012.

[3] K. R. Catchpole, S. Mokkapati, F. Beck, E. C. Wang, A. McKinley, A. Basch, and J. Lee, "Plasmonics and nanophotonics for photovoltaics," *MRS Bull.*, vol. 36, no. 6, pp. 461–467, 2011.

[4] I. Massiot, N. Vandamme, N. Bardou, C. Dupuis, A. Lemaître, J. F. Guillemoles, and S. Collin, "Metal Nanogrid for Broadband Multiresonant Light-Harvesting in Ultrathin GaAs Layers," *ACS Photonics*, vol. 1, no. 9, pp. 878–884, 2014.

[5] Y. Wang, T. Sun, T. Paudel, Y. Zhang, Z. Ren, and K. Kempa, "Metamaterial-plasmonic absorber structure for high efficiency amorphous silicon solar cells," *Nano Lett.*, vol. 12, no. 1, pp. 440–445, 2012.

[6] T. V. Pfeiffer, J. Ortiz-Gonzalez, R. Santbergen, H. Tan, A. Schmidt Ott, M. Zeman, and A. H. M. Smets, "Plasmonic nanoparticle films for solar cell applications fabricated by size-selective aerosol deposition," *Energy Procedia*, vol. 60, no. C, pp. 3–12, 2014.

[7] X. Guo, L. Liu, Z. Zhuang, X. Chen, M. Ni, Y. Li, Y. Cui, P. Zhan, C. Yuan, H. Ge, Z. Wang, and Y. Chen, "A New Strategy of Lithography Based on Phase Separation of Polymer Blends," *Sci. Rep.*, vol. 5, pp. 1–12, 2015.

[8] A. Mellor, N. P. Hylton, H. Hauser, T. Thomas, K.-H. Lee, Y. Al-Saleh, V. Giannini, A. Braun, J. Loo, D. Vercruysse, P. Van Dorpe, B. Blasi, S. A. Maier, and N. J. Ekins-Daukes, "Nanoparticle Scattering for Multijunction Solar Cells: The Tradeoff between Absorption Enhancement and Transmission Loss," *IEEE J. Photovoltaics*, vol. 6, no. 6, pp. 1678–1687, 2016.

[9] C. E. R. Disney, S. Pillai, and M. A. Green, "The Impact of parasitic loss on solar cells with plasmonic nano-textured rear reflectors," *Sci. Rep.*, vol. 7, no. 1, pp. 1–10, 2017.

[10] K. M. McPeak, S. V. Jayanti, S. J. P. Kress, S. Meyer, S. Iotti, A. Rossinelli, and D. J. Norris, "Plasmonic films can easily be better: Rules and recipes," *ACS Photonics*, vol. 2, no. 3, pp. 326–333, 2015.

[11] Y. Jiang, S. Pillai, and M. A. Green, "Realistic Silver Optical Constants for Plasmonics," *Sci. Rep.*, vol. 6, no. 1, p. 30605, 2016.

[12] P. B. Johnson and R. W. Christy, "Optical constants of the noble metals," *Phys. Rev. B*, vol. 6, no. 12, pp. 4370–4379, 1972.

[13] W. R. Erwin, H. F. Zarick, E. M. Talbert, and R. Bardhan, "Light trapping in mesoporous solar cells with plasmonic nanostructures," *Energy Environ. Sci.*, vol. 9, no. 5, pp. 1577–1601, 2016.

[14] P. R. West, S. Ishii, G. V. Naik, N. K. Emani, V. M. Shalaev, and A. Boltasseva, "Searching for better plasmonic materials," *Laser Photonics Rev.*, vol. 4, no. 6, pp. 795–808, 2010.

[15] E. D. Palik, *Handbook of Optical Constants of Solids*. Academic Press, 1985.

[16] T. A. F. Konig, P. A. Ledin, J. Kerszulis, M. A. Mahmoud, M. A. El-Sayed, J. R. Reynolds, and V. V. Tsukruk, "Electrically tunable plasmonic behavior of nanocube-polymer nanomaterials induced by a redox-active electrochromic polymer," *ACS Nano*, vol. 8, no. 6, pp. 6182–6192, 2014.

[17] K. C. Johnson, "GD-Calc.pdf," 2005. [Online]. Available: http://kjinnovation.com/GD-Calc.html.

[18] NREL, "Reference Solar Spectral Irradiance: Air Mass 1.5." [Online]. Available: http://rredc.nrel.gov/solar/spectra/am1.5/. [Accessed: 04-Aug-2017].

[19] H.-J. Hagemann, W. Gudat, and C. Kunz, "Optical constants from the far infrared to the x-ray region: Mg, Al, Cu, Ag, Au, Bi, C, and Al_2O_3," *J. Opt. Soc. Am.*, vol. 65, no. 6, p. 742, 1975.

[20] D. W. Lynch, C. G. Olson, and J. H. Weaver, "Optical properties of Ti, Zr, and Hf from 0.15 to 30 eV," *Phys. Rev. B*, vol. 11, no. 10, pp. 3617–3624, May 1975.

[21] R. L. Olmon, B. Slovick, T. W. Johnson, D. Shelton, S. H. Oh, G. D. Boreman, and M. B. Raschke, "Optical dielectric function of gold," *Phys. Rev. B - Condens. Matter Mater. Phys.*, vol. 86, no. 23, pp. 1–9, 2012.

[22] A. D. Rakić, A. B. Djurišić, J. M. Elazar, and M. L. Majewski, "Optical properties of metallic films for vertical-cavity optoelectronic devices," *Appl. Opt.*, vol. 37, no. 22, p. 5271, 1998.

[23] W. S. M. Werner, K. Glantschnig, and C. Ambrosch-Draxl, "Optical constants and inelastic electron-scattering data for 17 elemental metals," *J. Phys. Chem. Ref. Data*, vol. 38, no. 4, pp. 1013–1092, 2009.

[24] M. N. Polyanskiy, "Refractive index database." [Online]. Available: https://refractiveindex.info.